DESIGN OF A BETA-RAY-EXCITED HOMOGENEOUS X-RAY SOURCE FOR INDUSTRIAL APPLICATIONS

by

Thomas Fredrick Lagier

A Thesis Submitted to the
Graduate Faculty in Partial Fulfillment of
The Requirements for the Degree of
MASTER OF SCIENCE

Major Subject: Nuclear Engineering

Approved:

Signatures have been redacted for privacy

Iowa State University
Of Science and Technology
Ames, Iowa

1963

TABLE OF CONTENTS

INTRODUCTION

Isotopic sources of secondary low-energy radiation are currently being applied to an increasing number of industrial and research problems. Some of these applications are density and thickness gaging, energy reference sources for calibration, radiography of thin sections, and analysis of materials by critical absorptivity.

The need for development of isotopic sources of radiation has arisen from the fact that few suitable gamma emitting isotopes exist which produce gamma radiation in the energy region from a few Kev to several hundred Kev. While X-ray machines can provide beams of radiation in this energy region, they are costly, cumbersome, and hard to adapt to many practical applications. The advantages of isotopic sources of radiation are: compactness, portability, zero power requirement, and low cost.

The objective of this study is to design an isotopic source of secondary radiation which will produce a useful radiation beam covering a range of energies. Special efforts will be made to maintain the homogeneity of the desired energy radiation output.

REVIEW OF LITERATURE

Theoretical and empirical treatments of the interactions of particulate and electromagnetic radiation with matter have been presented by Evans (5), Kaplan (10), Segrè (17), and Siegbahn (18). Fano (6) has classified the possible interactions of electromagnetic radiation with matter into twelve basic processes, some of which have yet to be observed. Crouthamel (3) has edited a compilation of the gamma-ray spectra of a number of materials plus a tabulation of the characteristic X-ray emission energies of all elements. Burtt (1) has discussed the effects of geometrical arrangements upon beta detection methods, and Rockwell (16) has edited an extensive guide to shielding calculations for odd-geometry systems.

There are numerous sources of data which list the X-ray attenuation coefficients of materials. Davisson and Evans (4) have tabulated gamma-ray attenuation coefficients for a number of materials as functions of energy. Two of the more recent and inclusive sources of data on this subject are the works of Grodstein (9) and McGinnies (14) in which theoretical and experimental X-ray attenuation coefficients are given for 29 materials in the energy range from 10 Kev to 100 Mev.

During the last ten years a considerable number of experimental investigations of isotopic sources of radiation have been conducted. Cameron and Rhodes (2) investigated the use of Krypton-85 to excite characteristic radiation in a number of materials. An extensive study conducted by the Armour Research Foundation resulted in the reports of Filosofo (7), Reiffel (15), Voyvodic (20), and Voyvodic and Stone (21)

in which a number of sources and target materials were investigated. Leboeuf and Stark (12) conducted a basic investigation of the excitation of characteristic X-rays by beta particles. An experimental evaluation of the effects of bremsstrahlung upon the useful radiation output of a transmission type device has been conducted by Starfelt et al. (19) for various target thicknesses. The results of this investigation have been found to be of considerable value in the design.

THEORETICAL CONSIDERATIONS

Beta Rays and Their Interactions with Matter

Spectral distributions of beta rays

Radioactive nuclides which follow beta decay schemes may emit either negatrons (e^-) or positrons (e^+) depending on whether the given nuclide is proton or neutron rich. Positron decay is always accompanied by electromagnetic radiation. Negatron decay is often accompanied by gamma radiation; however, some pure beta emitters do exist which only emit negatrons in the decay process. In this design, considerations will be confined to negatron emitters. The equation for beta decay is

$$ {}_{Z}X^{A} \longrightarrow {}_{Z+1}Y^{A} + {}_{-1}e^{0} + \text{neutrino} \qquad (1) $$

Beta particles can be emitted having any kinetic energy from essentially zero to a maximum equal to the energy difference between the parent and product nuclei. Thus each beta source has its own characteristic end-point energy E_{max}. The spectral distribution of beta particles over this energy range is continuous with a predominance of beta particles being in the low-energy portion of the spectrum. It has been found by experiment that the average beta-ray energy of such a spectrum is about 0.3 E_{max}. It has also been found that the spectral distribution of beta rays is independent of the age of the source.

In addition to the continuous spectrum emitted in the decay process, some sources also exhibit secondary spectra which are due to extra nuclear electrons being ejected from the atom by a process called internal

conversion. A nucleus in an excited state can pass to a lower energy state of the same nucleus either by emitting a gamma ray or by imparting energy directly to a K or L shell electron. If the nucleus interacts directly with one of its orbital electrons, the electron is ejected from its shell with a kinetic energy equal to the difference in energy of the nuclear states minus the binding energy of the electron. Thus internal conversion electrons are emitted at single energies, and a line spectrum is superimposed on the continuous beta spectrum of a source subject to internal conversion processes.

Attenuation of beta rays

As a swift-moving electron traverses an absorbing medium, it is deflected many times from its original path by elastic and inelastic collisions with atomic electrons and nuclei. Its path through the medium is extremely crooked so that in being brought to rest the actual distance traveled by the electron may be considerably greater than the depth of penetration into the absorber. Evans (5) has estimated that the ratio of the actual path length to the thickness of the absorber penetrated may vary from 1.2 to 4.0, with the largest value being for slow-moving electrons traversing a high Z medium.

Beta-ray spectra are attenuated almost exponentially with increasing absorber thicknesses. This exponential decrease in numbers of particles penetrating absorber thicknesses continues until the maximum range of the beta spectrum is reached. At this point, the beta-ray transmission drops to zero. Many empirical expressions have been developed for the maximum range of a beta spectrum. The range is usually expressed in terms of the

end-point energy of the spectrum E_{max}. The expression given by Evans (5) for the energy range from 1.0 Mev to 20.0 Mev is

$$R = 530\ E_{max} - 106 \qquad (2)$$

The range is given in units of milligrams per cm^2 (mg/cm^2), and E_{max} is the end-point energy of the beta spectrum.

It has been found that the mass absorption coefficient for a beta-ray spectrum is nearly independent of the atomic weight of the absorber, rising slightly with increasing Z. The mass absorption coefficient seems only to be dependent on the end-point energy of the spectrum and is usually expressed in terms of this variable alone.

Interactions of beta rays with matter

Swift-moving electrons may lose kinetic energy or be deflected from their original paths by four principal types of interactions.

Inelastic collisions with atomic electrons Inelastic collisions with bound atomic electrons are usually the predominant mechanism by which swift-moving electrons lose kinetic energy in an absorber. In each such collision one or more atomic electrons receive enough energy to be raised to an excited state (excitation) or, if the energy received is great enough, to an unbound state (ionization).

Inelastic collisions with nuclei When a swift-moving electron passes in the vicinity of a nucleus, it experiences an acceleration and is deflected. The deflection it experiences may cause a quantum of radiation to be emitted. Radiation of this origin is called bremsstrahlung. The emission of bremsstrahlung requires that the colliding particle lose

an amount of kinetic energy equivalent to the energy of the bremsstrahlung photon. In this type of collision with a nucleus it is also possible for the incident particle to raise the nucleus to an excited state. However, the probability of this type of interaction occurring is much less than the probability of bremsstrahlung emission.

Elastic collisions with atomic electrons Incident electrons may be elastically deflected in the field of atomic electrons of an atom. It is necessary for the kinetic energy of the incident particle to be very low for this type of interaction to occur in significant amounts. Energy and momentum are conserved in the collision, and the energy transfer is usually less than the minimum amount required to excite the atom.

Elastic collisions with nuclei Swift-moving electrons involved in elastic collisions with nuclei are deflected, but do not radiate energy or excite the struck nuclei. The incident electrons only lose the amount of kinetic energy required to conserve momentum during such collisions.

Beta particles passing through a medium may be involved in any one of these four types of interactions. The elastic collisions, per se, are not significant when considering X-ray production. The primary interactions which lead to the production of X-rays are inelastic collisions with atomic electrons which result in characteristic radiation and inelastic collisions with nuclei which result in bremsstrahlung. X-rays generated by these inelastic collisions originate from one of four processes.

External characteristic radiation As stated previously, characteristic radiation is generated when an atomic electron receives enough

energy to be raised to an excited or ionized state. When an atomic electron is removed from the K, L,...shell of an atom, an orbital electron from an outer shell fills the vacancy in the inner shell. When this occurs, a photon may be emitted having an energy equal to the difference in the energy states of the electron filling the vacancy. This radiation is characteristic of the atom being excited. External characteristic radiation occurs in atoms other than that from which the particular beta particle originated.

Internal characteristic radiation When a beta particle is emitted through the electronic cloud of its own atom, there is a small probability that it will be involved in an ionizing collision with one of the K, L,...shell electrons of its own atom. If ionization does occur, internal characteristic X-rays are produced. The probability of this interaction occurring is on the order of 10^{-4} per beta decay.

External bremsstrahlung When beta particles are involved in radiative collisions with atoms other than those from which they originated, the resulting radiation is called external bremsstrahlung.

Internal bremsstrahlung Beta particles passing through the fields of the atoms from which they originated generate a continuous spectrum of internal bremsstrahlung. This radiation is attributed to the sudden change in nuclear charge which occurs when a beta ray is emitted from a nucleus. Evans (5) has estimated that about 1/137 quantum of internal bremsstrahlung is emitted per beta decay.

Of the four types of X-ray-producing interactions of beta rays with matter, external characteristic radiation production and external brems-

strahlung production are by far the most predominant. In practical applications, the effects of internal characteristic radiation and internal bremsstrahlung can be neglected as will be the case for the remainder of this design.

Characteristic radiation production

Inelastic collisions of charged particles with atomic electrons are usually divided into two classes, depending on the amount of energy transferred in the collision. If the binding energy of the struck electron is significant relative to the energy being transferred during the collision, then the interaction is termed a soft collision. If the energy transferred in the collision is large enough so that the struck electron can be regarded as being initially in a free state, then the interaction is termed a hard collision. If Q is the energy transferred in a collision, the limits for soft collisions are $Q_{min} \leq Q \leq H$, and the limits for hard collisions are $H \leq Q \leq Q_{max}$. The restriction placed on H is that it be large compared with the binding energy of the struck electron. Q_{min} is of the order of an excitation energy of one atomic electron, and Q_{max} is the maximum energy that can be transferred during any collision, i.e., a head-on collision.

For a beta particle with kinetic energy T involved in a hard collision with an atomic electron, the energy of the struck electron after the collision will be Q and the energy of the colliding electron will be T - Q. After the collision it is impossible to determine which one was the incident electron. Evans (5) confronts this situation by proposing that the faster electron after the collision shall be defined as the

incident electron insofar as future collisions are concerned. This in effect imposes the restriction that the maximum energy that can be transferred during an electron-electron collision is T/2. Therefore, using the definition of Evans,

$$Q_{max} = T/2 \tag{3}$$

The kinetic energy lost per unit path length due to ionizing collisions $(dT/ds)_{ion}$ is equal to the sum of the energies lost per unit path length in soft and hard collisions.

$$(dT/ds)_{ion} = (dT/ds)_S + (dT/ds)_H \tag{4}$$

Through detailed quantum-mechanical calculations of the energy lost by moving charged particles to bound electrons, Bethe developed a theory for the energy lost in soft collisions and later extended it to the case of particles having relativistic velocities. Bethe's theory expressed in terms of electron-electron collisions is

$$(dT/ds)_{Bethe} = \frac{2\pi e^4}{m_o v^2} NZ \left[\ln\left(\frac{2m_o v^2 H}{J^2[1-\frac{v^2}{c^2}]} \right) - v^2/c^2 \right] \tag{5}$$

where J represents the geometric mean of all of the ionization and excitation potentials of the absorbing atom. It has been found that J is approximately proportional to Z.

Except for extreme relativistic energies, a good approximation for the total energy lost in ionizing collisions is obtained by extending $(dT/ds)_S$ to include the region of hard collisions, i.e.,

$Q_{min} \leq Q \leq T/2$. Evans (5) has stated that this approximation is accurate within experimental error except for extremely relativistic electrons. Therefore, extending Equation 4 over these new limits gives

$$\left(\frac{dT}{ds}\right)_{ion} = \frac{2\pi e^4}{m_o c^2(v^2/c^2)} NZ \left[\ln\left(\frac{m_o c^2(v^2/c^2)T}{J^2(1 - v^2/c^2)}\right) - \frac{v^2}{c^2}\right] \qquad (6)$$

Therefore, for a given kinetic energy, the ionization losses of incident electrons vary almost directly with NZ, the electron density of the absorber. For increasing energies, the ionization losses per unit path length will decrease, except at very relativistic energies where the logarithmic term dominates. This high-energy variation is subject to question since, as stated previously, the approximation is invalid at extreme relativistic energies. Thus in the energy domain of beta-emitting nuclides, the largest ionization losses will occur when low-energy beta rays penetrate a high-electron-density absorber. In this energy region, Equation 6 can be approximated by the proportionality

$$(dT/ds)_{ion} \propto \frac{NZ}{(m_o c^2)(v^2/c^2)} \qquad (7)$$

Equation 6 expresses the energy lost by the incident particles, not the characteristic radiation produced by their interactions with the absorbing medium. Most of the collisions of an incident ionizing particle will be soft collisions in which only a small amount of energy is transferred to the struck atomic electron. Although hard collisions are infrequent, they can account for up to one-half of the energy of the incident electron as shown by Equation 3.

When an atomic electron has been removed from its electron shell, an outer electron fills the vacancy and returns the excited atom to its ground state. The electron filling the vacancy is transferred to a more negative energy state, and this excess energy is dissipated either by emission of a photon or by transferring the energy directly to an outer electron. If the latter case occurs, the electron receiving the energy is ejected from the atom. These energetic electrons are called Auger electrons.

For ionizations that occur in the K shell of an atom, the ratio of the number of K X-rays emitted to the number of primary K shell vacancies created per unit time is called the K fluorescence yield, W_k. The fluorescense yield of other shells is not well known. Crouthamel (3) has summarized various experimental data in a graph showing the variation of W_k with atomic number. W_k increases from very low values for low Z elements to almost unity for high Z elements. For elements of lead and above, W_k is often considered unity.

Bremsstrahlung production

Inelastic collisions, or radiative collisions, of electrons with nuclei result in the production of bremsstrahlung which is emitted in a continuous spectrum. When an electron passes in the vicinity of a nucleus and is deflected, it may radiate any amount of energy from zero up to its total kinetic energy T. Thus the maximum energy of a bremsstrahlung spectrum is equal to the maximum kinetic energy of the electrons involved in radiative collisions.

Classical theory predicts that a charged particle will radiate energy

every time that it is accelerated. On the other hand, quantum mechanics predicts a small probability of photon emission each time the charged particle is accelerated in the field of a nucleus; however, this probability is so small that usually no photon is emitted. When a collision is accompanied by photon emission, a large amount of energy is usually radiated. Experimental observations have confirmed the quantum-mechanical model, although the average total energy losses from the two theories are about the same according to Evans (5).

It has been determined from quantum mechanics that the total energy loss per unit path length due to radiative collisions of electrons is

$$(dT/ds)_{rad} = N(T + m_o c^2)\ \sigma_{rad} \tag{8}$$

where σ_{rad} (cm^2/atom) is the bremsstrahlung cross section. In the case of nonrelativistic electrons, i.e., $T \ll m_o c^2$

$$\sigma_{rad} = \frac{16}{3}\ \sigma_o\ Z^2 \tag{9}$$

where $$\sigma_o = \frac{1}{137}\left(\frac{e^2}{m_o c^2}\right)^2$$

No expression has been given for the moderately relativistic case of $T = m_o c^2$.

For the case of beta rays from most beta-emitting nuclides, the energy regions of interest would be confined between the nonrelativistic and moderately relativistic cases. Therefore, the energy losses due to

radiative collisions can be expressed in the proportionality

$$(dT/ds)_{rad} \propto \frac{NZ^2(T + m_oc^2)}{(m_oc^2)^2} \tag{10}$$

Thus it is seen that the energy loss is proportional to Z^2, while in the case of ionization losses it was proportional to Z. If T is small compared to m_oc^2, then the energy losses are approximately independent of T, the kinetic energy of the colliding particle. As T becomes large, the energy losses increase with the total energy of the colliding particle. Thus it is seen from Equation 10 that the greatest energy losses due to radiative collisions occur when high-electron-density materials absorb high-energy beta rays.

By utilizing Equation 7 and Equation 10, it is possible to evaluate the ratio of the energy losses for the two types of interactions. This ratio can be shown as

$$\frac{(dT/ds)_{rad}}{(dT/ds)_{ion}} \propto \frac{(T + m_oc^2)(v^2/c^2)Z}{m_oc^2} \tag{11}$$

Paul and Steinwedel in Siegbahn (18) have estimated the value of this ratio in the relativistic region, i.e., $v^2/c^2 = 1$, to be

$$\frac{(dT/ds)_{rad}}{(dT/ds)_{ion}} = \frac{(T + m_oc^2)Z}{1600\ m_oc^2} \tag{12}$$

Thus it is seen that the ratio of radiation losses to ionization losses can become significant. In the case of two Mev electrons penetrating a lead target, the energy losses due to radiative collisions are

about 25 percent of the losses due to ionization collisions.

Bremsstrahlung spectrums have been found to possess large intensities of low-energy photons, decreasing non-linearily with increasing energy to a maximum photon energy equal to the end-point energy of the beta spectrum generating the bremsstrahlung. It has been found that there is no dependence between the atomic number of the absorber and the shape of the bremsstrahlung spectrum produced. Thus each beta-emitting source has its own characteristic external bremsstrahlung spectrum.

Interactions of Electromagnetic Radiation with Matter

Interactions of electromagnetic radiation with matter are primarily dependent upon the energy of the radiation and the type of material absorbing the radiation. There are a number of interactions which can lead to the scattering or absorption of electromagnetic radiation. However, it has been found that in the energy region from a few Kev to ten Mev the greatest number of interactions are due to three processes: photoelectric effect, scattering by atomic electrons, and pair production.

Photoelectric effect

Photoelectric absorption results when an incident photon is absorbed by a bound atomic electron. In order for the photon to be completely absorbed, the electron must be bound to the atom so that momentum is conserved in the process by the recoil of the struck atom. The tightest-bound electrons have the greatest probability of completely absorbing a photon incident upon an atom. It has been determined that about 80 percent of all photoelectric absorptions occur in the K shell of the atom,

providing the energy of the photon exceeds the K absorption edge of the atom.

In the photoelectric process, an incident photon with energy H collides with a bound electron whose binding energy is B_e. The electron is ejected from its orbit with a kinetic energy T.

$$T = h\nu - B_e \tag{13}$$

This photoelectron can itself produce electromagnetic radiation by interactions as previously discussed. When the photoelectron is emitted, the struck atom is in an excited state as a result of the vacancy left in its electron shell. This vacancy is filled by an outer electron. Since the electron filling the vacancy comes from a higher energy level (less negative), the excess energy due to its transition is dissipated either by characteristic photon emission or Auger electrons, as discussed previously.

The probability that photoelectric absorption will occur is given by the atomic cross section ${}_a\tau$ (cm^2/atom). Evans (5) states that ${}_a\tau$ can be approximately evaluated as

$${}_a\tau \propto \frac{Z^n}{(h\nu)^m} \tag{14}$$

In the energy region from 0.1 Mev to 3.0 Mev, n increases in value from a number greater than four to a number less than five with increasing photon energy. In this same energy region, m takes integral values of one, two, or three as the photon energy is decreased. Thus the atomic number of the absorber has a very large influence on the photoelectric

cross section. Below the 0.1 Mev energy level, photoelectric cross sections are complicated by the discontinuities at the absorption edges. Above the absorption edges, photoelectric cross sections decrease rapidly with increasing photon energy.

Scattering by atomic electrons

Scattering of photons by atomic electrons can be separated into coherent scattering (Rayleigh scattering) and incoherent scattering (Compton scattering).

Coherent scattering predominates at low photon energies where the wave length of the photons is comparable to the dimensions of the atoms being struck. The photons are scattered from their original directions, but they do not lose any measurable amounts of energy in the process. In order for the photon to be scattered without losing significant amounts of energy, the energy received by the struck atom must be less than that required to cause excitation. The effect of this type of collision is that the photon collides elastically with the whole atom and is scattered through a small angle. Fano (6) has summarized Rayleigh-process deflections for aluminum, iron, and lead. This type of scattering is more likely to occur in high Z materials than in low Z materials.

Incoherent or Compton scattering occurs at photon energies which are large compared to the binding energies of atomic electrons. In this situation, the electron is considered to be initially free and at rest so that the scattering collision is treated as being elastic. Expressions for the energy of the scattered photon and electron are found by applying conservation of energy and momentum to the scattering process.

Since a Compton collision is elastic, no radiation is generated during the collision. However, the scattered electron is capable of producing radiation by the interactions discussed earlier, and the decrease in energy of the scattered photon will increase the probability of the photon being absorbed by a photoelectric interaction. Therefore, Compton collisions are important in this design in that the products of such collisions will produce radiations that may affect the spectral distribution of the useful radiation output.

The cross section for Compton scattering has been calculated by Klein and Nishina using a quantum-mechanical treatment. The total Compton cross section ${}_e\sigma$ is the cross section for removal of photons from the original beam and can be expressed as

$$ {}_e\sigma = 2\pi\,(e^2/m_o c^2)\left[\frac{1}{\alpha^3}\ln(1+2\alpha) + \frac{2(1+\alpha)(2\alpha^2-2\alpha-1)}{\alpha^2(1+2\alpha)^2} + \frac{8\alpha^2}{3(1+2\alpha)^2}\right] \tag{15} $$

where $$ \alpha = \frac{h\nu_o}{m_o c^2} $$

From this expression it is seen that Compton scattering is a function of photon energy only and decreases as the energy of the incident radiation is increased.

The total linear attenuation coefficient for Compton scattering is equal to the cross section per electron, ${}_e\sigma$, times the electron density of the absorber, NZ.

$$ \sigma = NZ\ {}_e\sigma \tag{16} $$

Thus the probability of Compton scattering occurring in an absorber is only dependent on the electron density of the absorber and the energy of the incident radiation. In the region of the absorption edge of an atom, Compton scattering is small compared to photoelectric absorption.

Pair production

Pair production can occur when a photon of sufficient energy passes through the field of a charged particle. In the process, the photon disappears and a positron-negatron pair is formed in its place. Since two particles are formed, each having a rest mass equal to $m_o c^2$, the minimum energy at which pair production can occur is equal to $2m_o c^2$ or 1.02 Mev. Any energy that the photon possesses above this amount will appear as kinetic energy of the positron-negatron pair. Expressed in notation form

$$h\nu = T_+ + T_- + 2m_o c^2 \qquad (17)$$

The negatron will interact with the absorber as previously described for swift-moving electrons. The positron will be slowed down by collisions with atoms until it is almost at rest; then it will interact with an electron. The two particles will be annihilated and two photons will be created moving in opposite directions, each having an energy of 0.51 Mev.

The probability of pair production occurring above 1.02 Mev increases with increasing photon energy. Davisson in Siegbahn (18) has summarized and compared pair production cross sections as calculated from several quantum-mechanical approaches. The results are not in complete agreement;

however, it is possible to see that pair production is strongly dependent upon the atomic number of the absorber and the energy of the incident radiation.

In this design, pair production could only occur by the interactions of high-energy bremsstrahlung. The magnitude of these interactions would be small for most beta sources.

Attenuation of electromagnetic radiation

As electromagnetic radiation passes through an absorber, the change of its intensity I per unit thickness of absorber traversed is proportional to the intensity of the radiation upon the unit thickness. Expressed in differential form

$$dI/dx = - \mu I \tag{18}$$

Integration of this expression yields the exponential relation

$$I = I_o e^{-\mu x} \tag{19}$$

where I_o is the intensity of radiation upon the absorber at $x = o$, I is the intensity at x, and μ is the attenuation coefficient. This is the fundamental equation for the attenuation of electromagnetic radiation in matter.

The attenuation coefficient is the summation of the attenuation coefficients for photoelectric absorption, scattering, and pair production. Since each of these quantities is energy dependent, μ will also be energy dependent. Therefore, Equation 19 can only be applied to radiation having the same energy as that at which μ is evaluated. The other

limitation placed on Equation 19 is that it is assumed that the incident beam is well collimated and that once a photon interacts with the absorber it is removed from the beam and does not return.

The attenuation coefficient used in Equation 19 can be expressed in a number of ways. Quite often a mass attenuation coefficient is used which is independent of the actual density or physical state of the absorber. The absorption coefficient for photoelectric absorptions can be expressed as

$$\mu = \frac{a\tau\ (cm^2/atom)\ N_{avo}(atoms/gram\ atom)}{A\ (grams/gram\ atom)} \qquad (20)$$

where N_{avo} is Avogadro's number, and A is the atomic weight of the absorber. When using a mass attenuation coefficient, the thickness of the absorber traversed is expressed as

$$t = x_{(cm)}\ \rho(g/cm^3) \qquad (21)$$

where x is the linear thickness of the absorber and ρ is the density. t is often referred to as the density thickness of the absorber.

DESIGN

A useful beam of X-radiation will be produced in this design by employing a transmission-reflection target configuration. Beta rays will be projected upon the transmission target, henceforth called the primary target, and will be converted into characteristic radiation and bremsstrahlung. This radiation will then be projected upon a reflection target, henceforth called the secondary target, where a portion of the impinging radiation spectrum will be absorbed in photoelectric interactions. It is the characteristic radiation produced in the secondary target which will be withdrawn for useful application. All radiation produced in the primary target having energies in the K-characteristic energy region of that target will be referred to as K_1 photons. K-characteristic radiation generated in the secondary target will be referred to as K_2 photons. In general, expressions associated with the interactions of K_1 photons will be written with the subscripts 1, and expressions associated with the interactions of K_2 photons will be written with the subscripts 2. Figure 1 shows the general source-target configuration which will be employed in this design and identifies the various parts of the device.

Source

As stated previously, bremsstrahlung is produced by the attenuation of all beta spectra. Since a large portion of a bremsstrahlung spectrum is in the low-energy photon region, proper choice of source and target can yield significant quantities of low-energy bremsstrahlung in the K_1

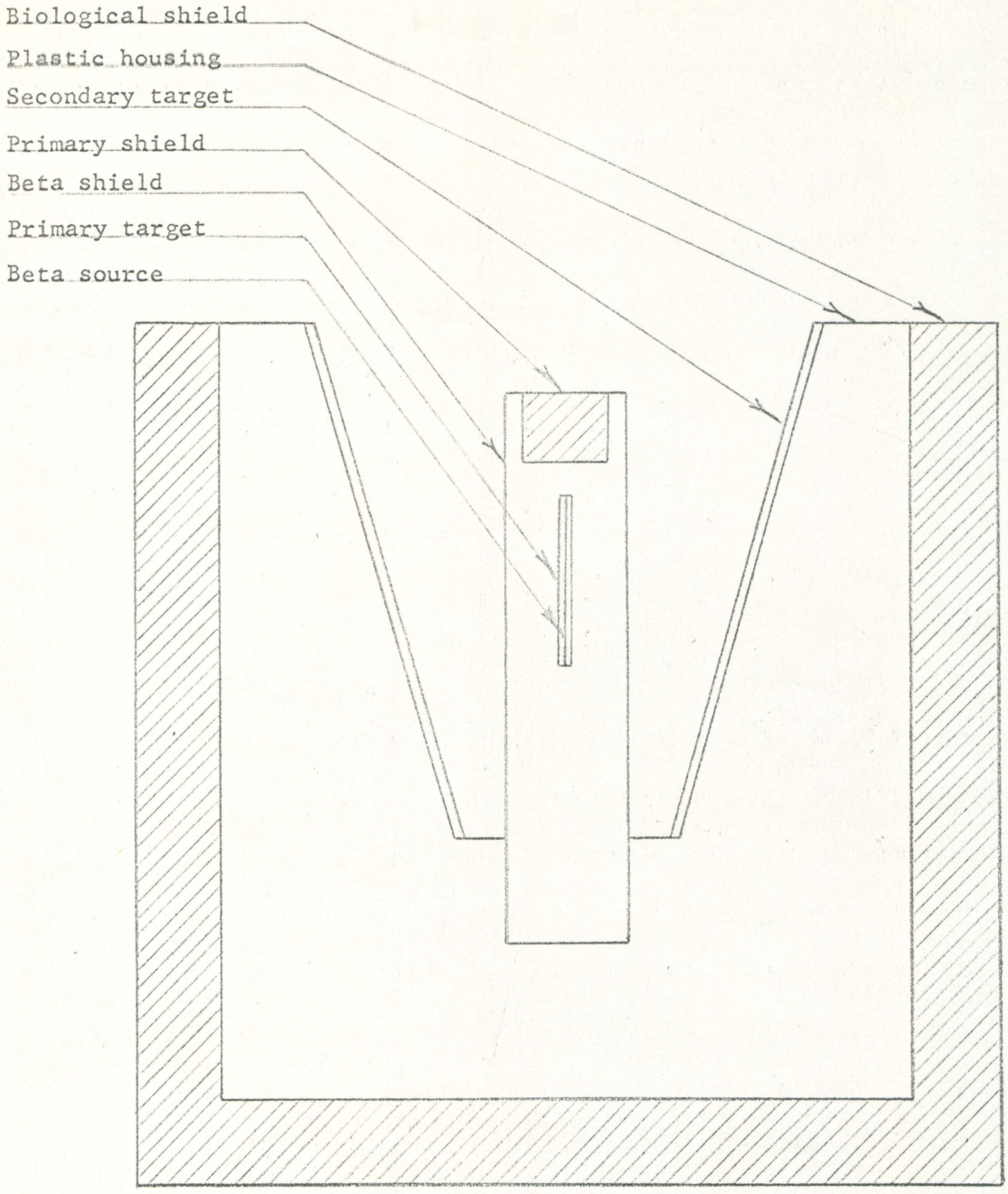

Figure 1. Geometrical arrangement of the X-ray device

photon energy region of the absorber. To accomplish this in an efficient manner, a high-energy beta source is required as shown by Equation 10.

Equation 7 shows that beta-ray energy losses due to excitation and ionization are inversely proportional to v^2/c^2. However, the majority of ionizing collisions experienced by a beta particle result in the transfer of only small amounts of energy. Only in a very few interactions will a given beta particle lose sufficient energy in the collisions with inner atomic electrons to result in the removal of the electron from the atom. At high energies the ionization energy losses do not decrease to zero, but approach an asymptotic value as v^2/c^2 approaches unity. Therefore, a high-energy beta spectrum would initially produce large amounts of bremsstrahlung. As the energies of these high-energy beta particles are decreased due to radiative collisions, the probability that ionizing collisions will occur is increased. Based on this analysis, a high-energy beta source will be utilized in this design.

The other requirements that must be considered when choosing the source are the availability, half-life, and radiation purity of the source. For practical applications, the source should be readily obtainable and have a reasonably long half-life. In addition, the source should not emit any high-energy gamma radiation which would adversely affect the purity of the useful radiation output.

Based on all of the above requirements, the source that has been chosen for this design is Sr^{90} - Y^{90}. The decay scheme for this material is

$$Sr^{90} \xrightarrow[t_{1/2} = 28\ yr]{\beta^-} Y^{90} \xrightarrow[t_{1/2} = 64\ hr]{\beta^-} Zr^{90}\ (stable) \qquad (22)$$

Sr^{90} emits a beta spectrum having an end-point energy of 0.544 Mev. Y^{90} emits a beta spectrum having an end-point energy of 2.23 Mev. A 1.75 Mev line spectrum of internal conversion electrons is emitted by Y^{90}; however, this only occurs in about 0.02 percent of Y^{90} decays. The potential health hazard presented by this material requires that special consideration be given to its containment.

The geometry of the source should permit a maximum number of beta rays to strike the primary target. Also, the source should be thin so that self-absorption in the source is small. These requirements can best be met by use of a line source which is completely surrounded by a uniform thickness of target material. Such a source configuration will be used in this design. By using essentially carrier-free material, a line geometry can be approximated quite well.

Equation 2 gives an empirical expression for the range of beta rays in an absorber. Good correlation has been found between this empirical expression and experimental observations. When this equation is evaluated for Sr^{90} - Y^{90}, the maximum range of the source is calculated to be 1080 mg/cm^2. This value will be used in the remainder of the calculations.

Primary Target

It was shown in Equation 7 that excitation and ionization energy losses are proportional to NZ, the electron density of the absorber. In Equation 10 it was found that radiative collision energy losses are proportional to NZ^2. Therefore, a high-atomic-numbered, dense material is required for the primary target in both the case of characteristic-

radiation production and bremsstrahlung generation. Two readily obtainable elements which meet this requirement are lead and uranium.

From previous considerations, it is to be expected that uranium would be more efficient than lead in converting the energy of the beta spectrum into K_1 photons. The primary disadvantages of uranium are the multiple gamma photons emitted in its decay scheme and the special precautions that must be taken when working with the metal. Most of the gamma radiation emitted by the decay chain of uranium is of sufficiently low energy to be adequately shielded from the detector. The use of uranium as a target material would extend the useful energy range of the device. The K_1 photons generated in an uranium target would be energetically capable of producing higher energy K_2 photons than would be the case with a lead target. Based upon these considerations, uranium will be the material used for the primary target. It will have the geometry of a cylinder and will surround the source with a uniform thickness of material.

Considerable experimentation has been done using lead as a target for beta rays, while very little experimental work has been reported using uranium. The two materials should not differ greatly in their responses to beta-ray interactions. Therefore, in order to utilize past experimental results for justification of portions of this design, theoretical analyses will be evaluated for lead and compared with experimental results for lead. Then the analyses will be evaluated for uranium and utilized in the design.

It was stated previously that beta-ray spectra are attenuated almost

exponentially over the greater portion of the range of the spectrum. Therefore, in a collimated beam, the number of unattenuated beta rays at any point in the primary target can be stated approximately as

$$B = B_o e^{-\mu_\beta t} \qquad 0 \leq t < R_{max} \tag{23}$$

where B_o is the number of beta rays in the source beam, μ_β is the attenuation coefficient of the source spectrum, and t is the thickness of absorber traversed.

As the beta rays interact with the absorber, photons are generated by the mechanisms discussed previously. If the target is thin, only a small number of photons will be generated. If the target is thick, a maximum number of photons will be generated, but many will be absorbed in the target. Therefore, it is necessary to optimize these two opposing processes in order to obtain the maximum net number of photons from the target. This optimization will be achieved by the following approximate analysis.

It will be assumed that a collimated beam of beta rays enter the primary target normal to its surface. The differential expression for the net rate of change of P_1 photons at any thickness t in the target is

$$dP_1/dt = Y\mu_\beta B - \mu_x P_1 \qquad 0 \leq t < R_{max} \tag{24}$$

where Y is the yield of P_1 photons per beta attenuation. Y is a function of beta-ray energy, target material, and generated photon energy. Since the X-ray attenuation coefficient μ_x is a function of target material and photon energy, the above expression is valid for a given energy only.

By integrating Equation 24 and applying the boundary condition that when $t = o$, $P_1 = 0$, the expression for the net number of P_1 photons emitted by the primary target per unit time is

$$P_1 = \frac{Y\mu_B B_o}{(\mu_B - \mu_x)} \left(e^{-\mu_x t} - e^{-\mu_B t}\right) \tag{25}$$

where t must be less than the range of the beta spectrum.

Since P_1 is initially an increasing function of target thickness, the maximum net number of photons are produced when the rate of change of P_1 with respect to t is zero. By applying this condition to Equation 24 and substituting Equations 23 and 25, the expression for optimum primary target thickness is

$$t_{opt} = \frac{1}{(\mu_B - \mu_x)} \ln (\mu_B/\mu_x) \tag{26}$$

Thus it is seen that the optimum target thickness is approximately determined by the attenuation coefficient for the beta spectrum and the X-ray attenuation coefficient of the absorber. Subsequent to making this analysis, it was found that Filosofo (7) has utilized essentially the same expression given by Equation 26 to calculate the optimum target thicknesses of several materials, although no general correlation with experimental data was made. Since it is desired to obtain a maximum number of K_1 photons from the primary target, μ_x will be evaluated at the energy of the K_1 photons, i.e., 98.0 Kev.

Grodstein (9) and McGinnies (14) have tabulated experimental and

theoretical absorption coefficients for various materials as a function of photon energy. The experimental data tabulated is quoted as being accurate within ten percent. In the characteristic X-ray region, most of the photon attenuation is due to photoelectric absorption. Coherent scattering becomes significant at very low energies, but since this type of interaction does not degrade the energy of the photons, its effect will generally be excluded from the calculations of this design. The data of the above authors will be used to evaluate all X-ray attenuation coefficients encountered in this design.

Various empirical expressions have been developed for the mass attenuation coefficient μ_B of beta spectra. As stated previously, μ_B has been found to be nearly independent of the atomic weight of the absorber and is usually expressed as a function of E_{max}. Evans (5), Kats and Penfold (11), and Gleason et al. (8) have presented expressions for μ_B fitted to various experimental data. The form of these equations differs only in the constants used. The equation developed by Gleason et al. is based on the most recent data and is given as

$$\mu_B = 17/E_{max}^{1.43} \qquad 0.15 \text{ Mev} < E_{max} < 3.5 \text{ Mev} \qquad (27)$$

This expression is only valid over the region of the beta absorption curve which is truly exponential. Approximate exponential attenuation occurs over the major portion of the range however, and Equation 27 can be used to evaluate the optimum thickness of the primary target. Sr^{90} has a considerably different mass attenuation coefficient than that of Y^{90}. It is impossible to optimize the primary target for both beta

spectra; therefore, the effect of the Sr^{90} will be neglected.

Evaluating Equation 27 for Y^{90} yields $\mu_g = 5.42\ cm^2/g$. Thus, for the source used in this design, the derived expression for optimum target thickness can be stated as

$$t_{opt} = \frac{10^3}{5.42-\mu_x} \ln (5.42/\mu_x) \qquad (28)$$

where t_{opt} is expressed as mg/cm^2. Figure 2 shows the variation of optimum target thickness with total X-ray attenuation coefficient for a Y^{90} beta source and is based on Equation 28. From the curve, the following optimum thicknesses are obtained: Sn, 128 mg/cm^2; U, 260 mg/cm^2; Pb, 265 mg/cm^2.

Filosofo (7) experimentally determined the following optimum target thickness for a Y^{90} beta source in a transmission geometry: Sn, 110 mg/cm^2; and Pb, 250 mg/cm^2. Lidén and Starfelt (13) concluded from their experiments that a 230 mg/cm^2 lead target produced the maximum net number of photons in the K X-ray region of the target when using a P^{32} source (E_{max} = 1.71 Mev).

As stated previously, considerable experimental work has been done using a lead transmission target. By substituting Equation 27 into Equation 26 and evaluating μ_x for a lead target, optimum lead target thickness as a function of the maximum energy of beta spectra can be stated as

$$t_{opt} = \frac{10^3}{(17/E_{max}^{1.43})-2.5} \ln (6.85/E_{max}^{1.43}) \qquad (28a)$$

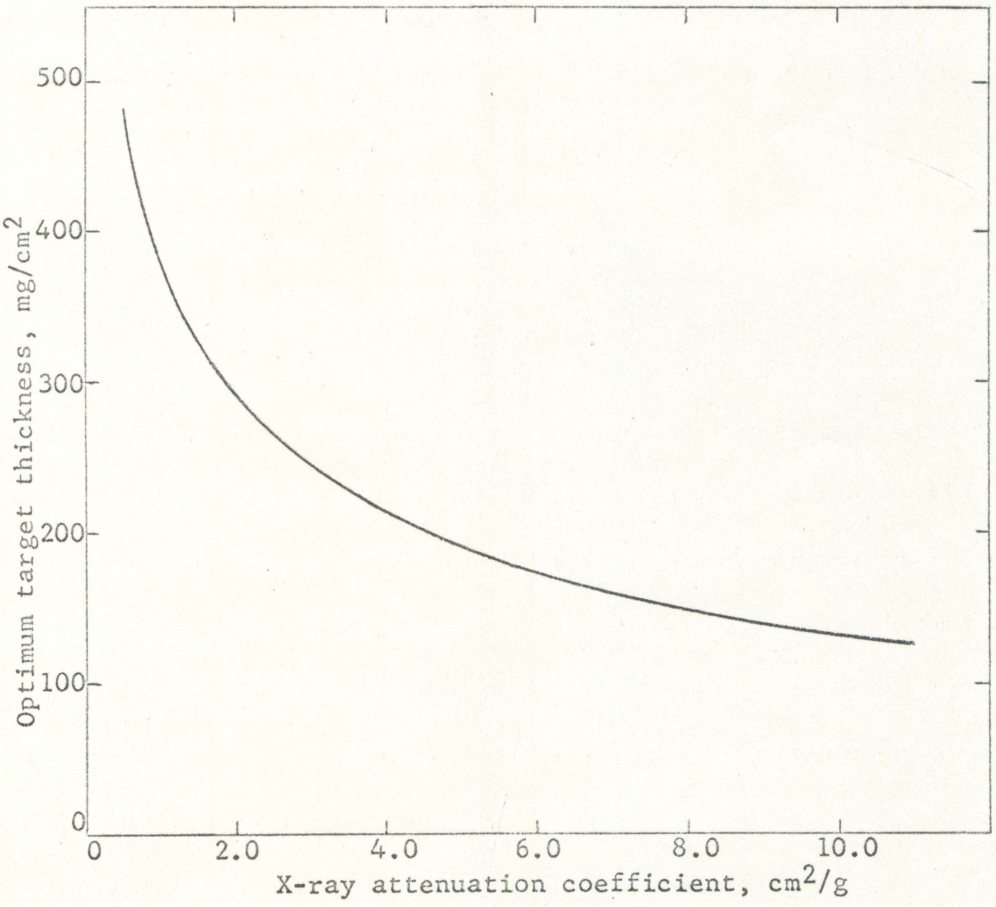

Figure 2. Optimum target thicknesses as a function of K-characteristic X-ray attenuation coefficients of materials

where E_{max} is expressed in Mev and t_{opt} in mg/cm^2. Figure 3 is a graph of Equation 28a from 0.2 Mev to 3.0 Mev. Six experimentally determined points are shown for comparison. The plotted function represents the experimental data quite well up through the energy corresponding to Y^{90}. Above this energy, Equation 28a appears to overestimate t_{opt}. In the experimental work conducted by Starfelt et al. (19) it was concluded that optimum target thickness increases slowly with E_{max} at low energies and levels off at a value of about 300 mg/cm^2 for end-point energies greater than 3.0 Mev.

Figure 4 is a plot of Equation 25 for a Y^{90} source and lead target showing the relative net distribution of K_1 photons in the target. Relative intensities are shown because of the complex nature of the factor Y. The analytical development of Y is a separate problem in itself. In comparing the shape of this curve with the experimental results of Filosofo (7) and Starfelt et al. (19), good correlation is found between the calculated and experimental cases. A similar curve for uranium would show about the same relative distribution because of the small difference in the characteristic X-ray attenuation coefficients of the two materials. It is seen from Figure 4 that the tolerance of the primary target is not as critical as might be expected when first considering the problem. Peak optimization would require a tolerance of $\pm$ 10 mg/cm^2 for a lead or uranium target; however, a tolerance of $\pm$ 50 mg/cm^2 could be allowed without seriously affecting the efficiency of K_1 photon generation in the target.

From the previous comparisons it is seen that the simplified repre-

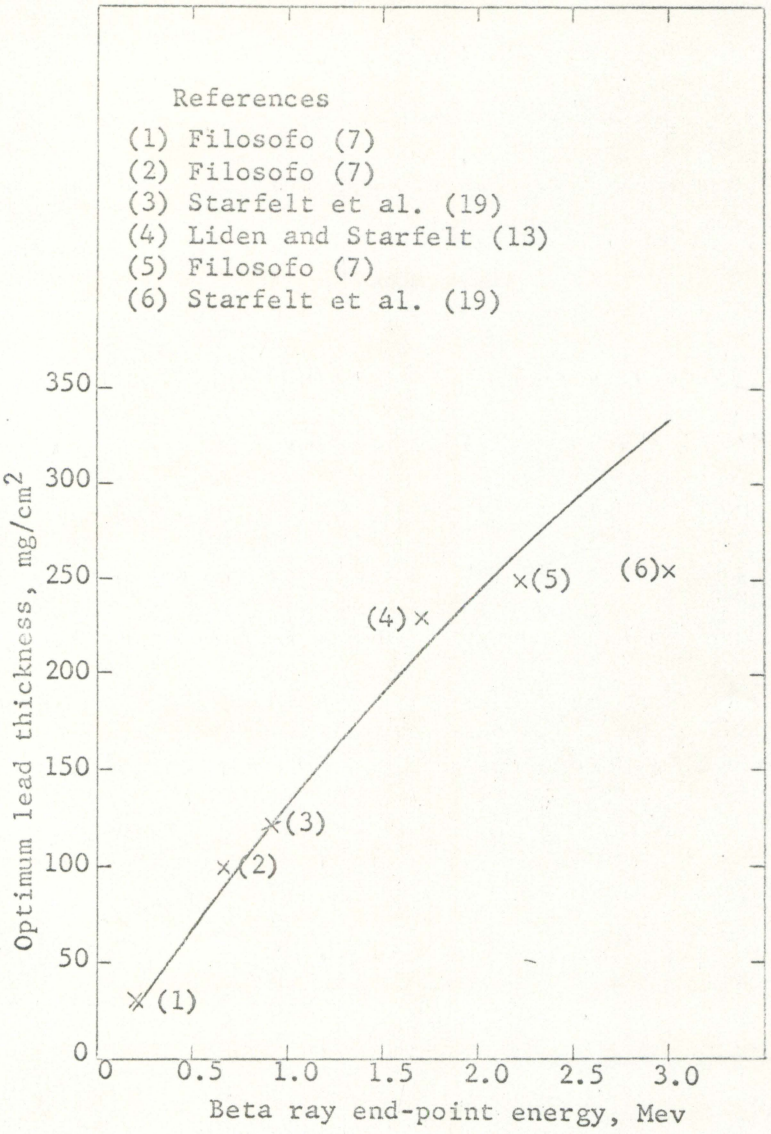

Figure 3. Optimum thicknesses of lead as a function of the end-point energies of beta-ray spectra

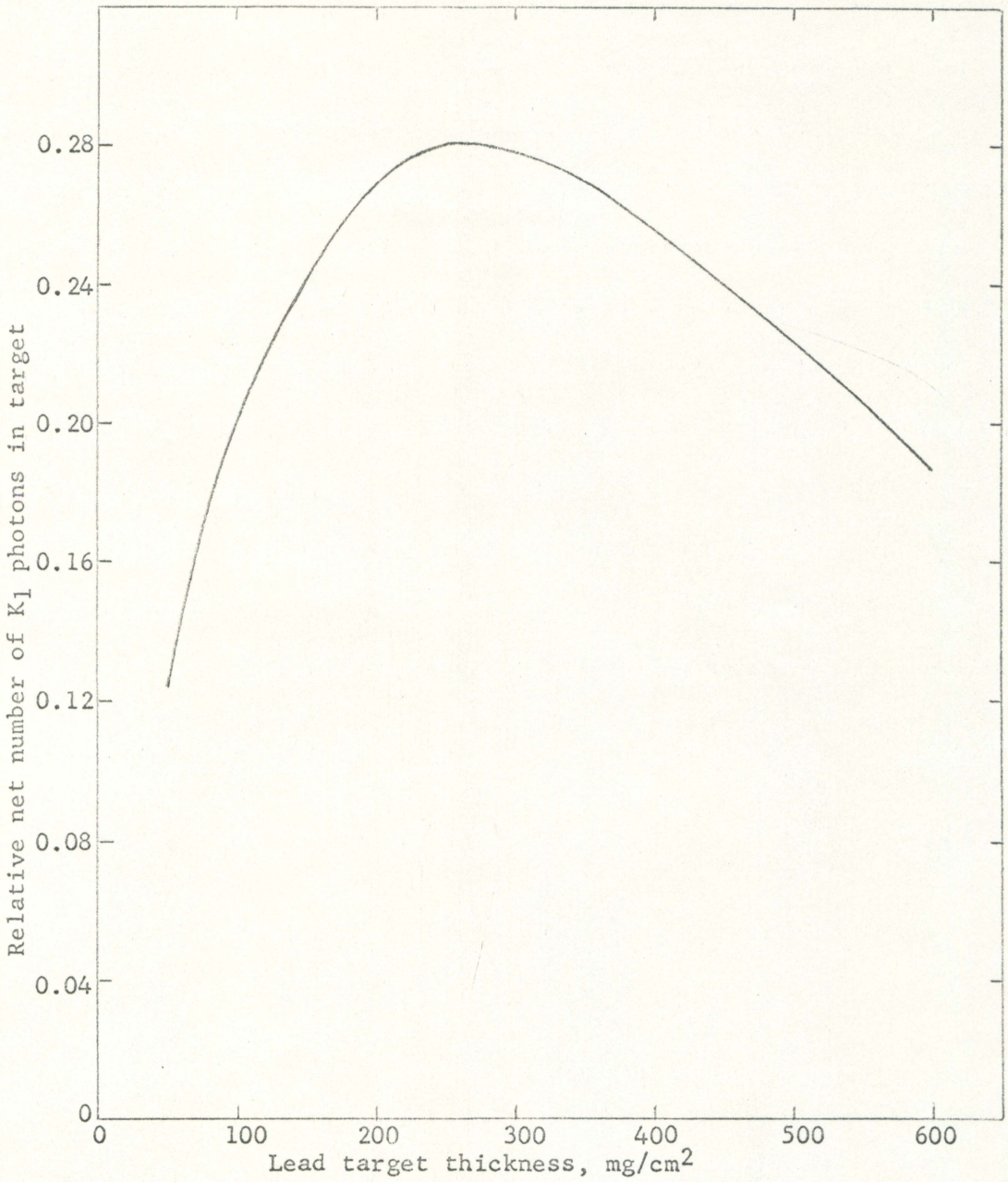

Figure 4. Relative K_1 photon distribution in a lead target using a Y^{90} source

sentation of the actual physical problem yields expressions which can be applied to most beta sources and to all target materials. Based on this analysis and the experimental results cited, the thickness of the primary target will be specified as 250 mg/cm^2 in this design.

The maximum range of beta rays from Sr^{90} - Y^{90} was calculated to be 1080 mg/cm^2. A primary target thickness of 250 mg/cm^2 will not prevent all of the particles from reaching the secondary target and generating additional radiation in that target. In order to maintain the radiation purity of the useful output of the device, a beta shield will be placed around the primary target and will be thick enough to prevent source beta particles from reaching the secondary target. In this design, the thickness requirement of the shield is 830 mg/cm^2.

Low Z materials have good X-ray transmission properties. Table 1 compares the transmission properties of three low Z materials in a beam of collimated K_1 photons.

Table 1. Transmission properties of low Z materials for K_1 photons

Element	μ_{K_1} (cm^2/g)	ρ (g/cm^3)	μ_{K_1} (cm^{-1})	t (cm)	I/I_o
Beryllium (Be)	0.13	1.84	0.239	0.452	0.898
Carbon (C)	0.15	2.10	0.315	0.396	0.883
Aluminum (Al)	0.16	2.70	0.433	0.308	0.875

In the above table, t is the thickness of material required to provide a density thickness of 830 mg/cm^2. I/I_o is the fraction of the K_1 photons that pass through the shield unattenuated, traveling normal to

its surface. It is seen from the table that beryllium would be the best shield material from the standpoint of radiation transmission. However, with the geometry being used, the greater thickness of beryllium would have a considerably greater shadowing effect between the secondary target and detector than would be the case for the aluminum shield. Therefore, an aluminum shield will be used in this design and will have a wall thickness of 830 mg/cm^2. This shield will also provide the necessary containment for the source and will be sealed with a lead plug which will shield undesirable radiation from the detector.

Both the beta shield and the geometrical configuration of the secondary target will have an effect upon the number of K_1 photons intercepted by that target. In order to determine the K_1 flux distribution ϕ^* along the surface of the secondary target, an exponential kernel method of calculation will be employed. Figure 5 is a scaled drawing of the device showing pertinent dimensions, and Figure 6 shows the notation which will be employed in the calculation of ϕ^*.

The probability that photons isotropically emitted by a point will reach a point d cm away from the source without being attenuated is

$$\frac{dA}{4\pi d^2} e^{-b} \tag{29}$$

where dA is the detector area seen by the source, d is the distance from the source to the detector, and b is the sum of the attenuation relaxation lengths between the source and detector. The expression for b is

$$b = \sum_{i=1}^{n} \mu_i t_i \tag{30}$$

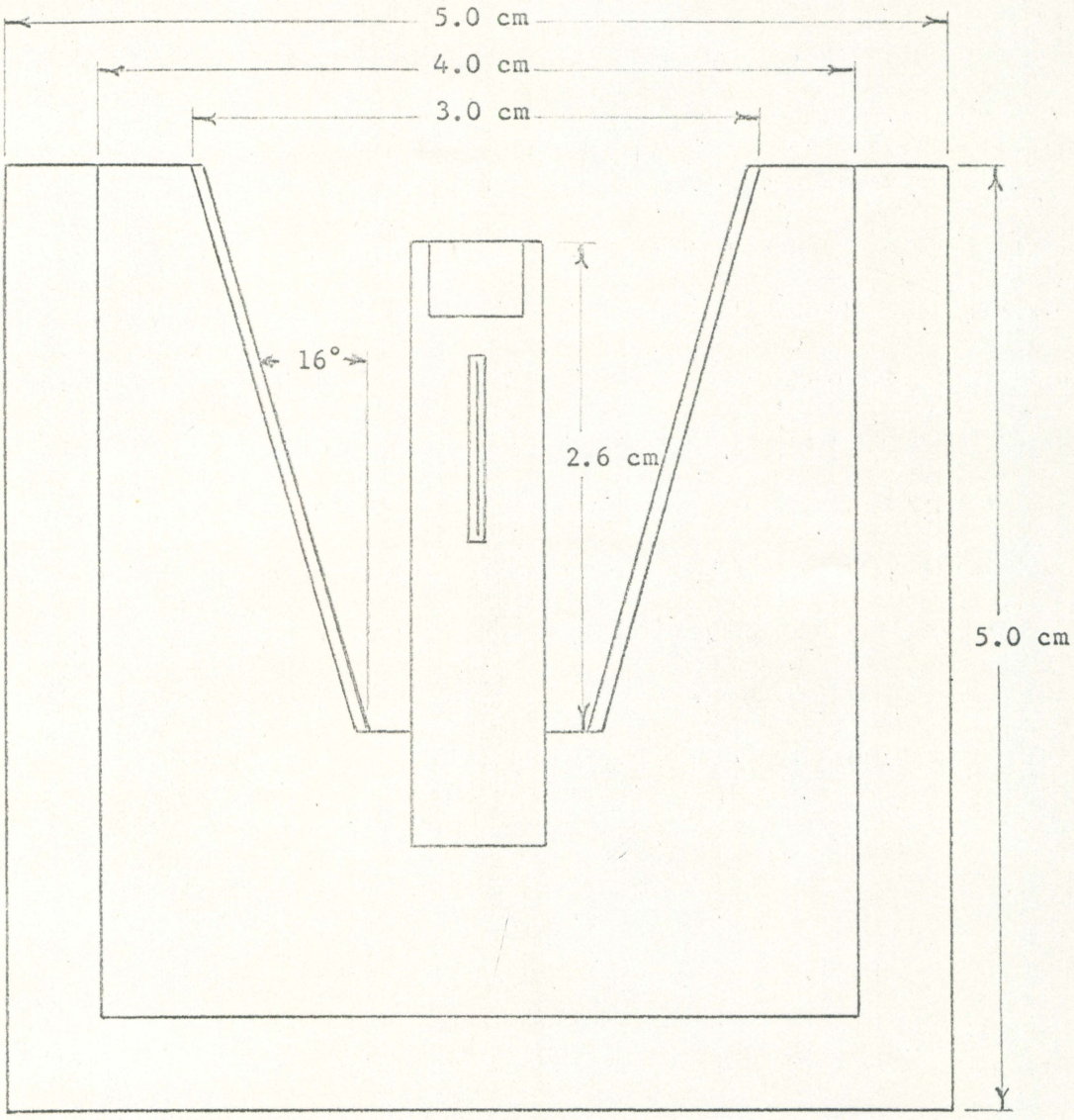

Figure 5. Scaled sectional view of the device. Scale: 1 inch = 1 centimeter

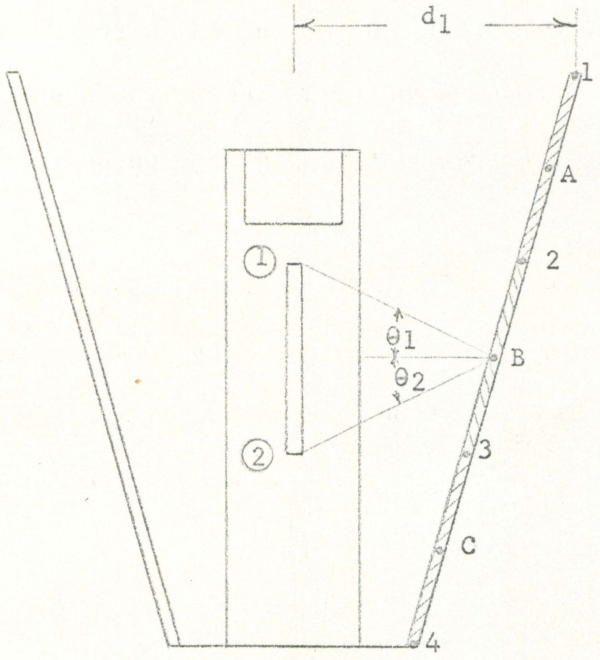

Figure 6. Evaluation points and area elements of secondary target

When the point kernel is applied to the line geometry shown in Figure 6

$$d\phi^* = \frac{S_L\, e^{-b \sec \theta}}{4\pi(d \sec \theta)}\, dl \qquad (31)$$

where S_L is the intensity of the line source per unit source length. The differential length of the source dl is related to dθ by

$$dl = d \sec^2 \theta\, d\theta \qquad (32)$$

When this expression for dl is substituted into Equation 31 integration of the resultant expression yields

$$\phi^* = S_L/4\pi d \left[\int_0^{\theta_1} e^{-b \sec \theta}\, d\theta + \int_0^{\theta_2} e^{-b \sec \theta}\, d\theta \right] \qquad (33)$$

The integrals in the above expression are evaluated graphically by Rockwell (16) as F(θ,b) functions. Therefore, the expression for ϕ^* can be given as

$$\phi^* = S_L/4\pi d \left[F(\theta_1,b) + F(\theta_2,b) \right] \qquad (34)$$

It is seen in Figure 6 that the quantity b is made up of a relaxation length due to the photon attenuation in the beta shield and also a relaxation length due to attenuation in the air between the shield and the secondary target. The attenuation effect of the air is so small that it can be neglected. By substituting the values for each of the points in Figure 6 into Equation 34, the following values are obtained for the K_1 photon flux along the surface of the secondary target.

$$\phi_1^* = 1.38 \times 10^{-2} S_L$$

$$\phi_A^* = 2.54 \times 10^{-2} S_L$$

$$\phi_2^* = 4.54 \times 10^{-2} S_L$$

$$\phi_B^* = 6.69 \times 10^{-2} S_L$$

$$\phi_3^* = 7.17 \times 10^{-2} S_L$$

$$\phi_C^* = 3.98 \times 10^{-2} S_L$$

$$\phi_4^* = 1.59 \times 10^{-2} S_L$$

In applying this method of evaluating ϕ^*, it must be kept in mind that the difference of the F(θ,b) functions is required when one of the angles is included in part of the other subtended angle. This situation occurs at point 1, A, C, and 4.

An average K_1 photon flux at the surface of the secondary target will be applied to a later portion of this design. The arithmetical average of the seven evaluated points will be taken since they are all equally spaced and the effect of air attenuation is negligible. Therefore, the average K_1 photon flux that can be applied to the secondary target is

$$\phi_{av}^* = 3.9 \times 10^{-2} S_L \qquad (35)$$

In experimental work reported by Starfelt et al. (19), it was found that for high energy beta sources and high Z targets of optimum thickness the K-energy photon yield per beta decay could be as high as 0.2. On the other hand, Filosofo (7) experimentally determined a K-energy photon yield per beta decay of 0.03 for a Y^{90} source and a lead target of optimum thickness. The discrepancies between these quoted values are largely attributed to the increased self-absorption which occurs in the

thicker sources. Since the beta-ray target in this design is uranium, a higher efficiency of conversion is to be expected than for the case of a lead target. Also, the beta source in this design is thin so that self-absorption in the source will be small. On this basis, the K_1 photon yield will be taken as 0.10 per beta decay in the following calculations. The expression for S_L in symbolic form is

$$S_L = 0.10\ C \tag{36}$$

where C is the Y^{90} activity of the source expressed as disintegrations per second per unit source length. As shown in Figure 5, the length of the source is 1.0 cm.

Secondary Target

The primary target has been optimized for the passage of 98 Kev X-rays. For K characteristic X-ray production in the secondary target, the K absorption edge of the target must be less than 98 Kev. All elements below radon in the periodic table meet this requirement. Thus, by proper choice of the secondary target material, it is possible for the device to generate a useful radiation output ranging from a few Kev to about 80 Kev. The heavier materials will be more efficient K_2 photon generators for two reasons: the K absorption edges of the heavier materials are closer to the energy of the incident radiation, and the fluorescence yield of high Z materials is greater than for the case of the lighter elements. Three materials will be evaluated as secondary targets in this design to provide a low, medium, and high energy output

from the device. These materials are listed in Table 2 along with some of their characteristics.

Table 2. Secondary target materials

Element	Z	$\rho(g/cm^3)$	K (Kev)	W_k
Tin (Sn)	50	7.18	25.3	0.82
Tungsten (W)	74	18.6	59.3	0.95
Lead (Pb)	82	11.0	75.0	0.96

The secondary target will have the shape of the surface of a frustum of a cone with the ends removed. It will be placed with its axis of symmetry coincident with the primary target as shown in Figure 5. The target will generate K_2 photons which will be emitted isotropically. It is those X-rays which are emitted back through the surface of the target upon which the incident beam entered which will constitute the useful radiation output of the device. This radiation is not collimated as it leaves the device.

For maximum K_2 photon generation, the secondary target should be infinitely thick. However, in this energy region, photon absorption probabilities are so high that an essentially infinite target thickness for K_2 photon generation will be achieved at a very small linear target thickness. For the geometry utilized in this design, thicknesses greater than the effective infinite amount would be of no value for additional K_2 photon production and actually would be detrimental due to the increased Compton scattering of the incident radiation.

The actual K_1 photon distribution at the surface of the secondary target is complicated by the additional scattering introduced by the beta shield. In order to arrive at a reasonable analysis of the secondary target, a simplified representation of the actual case will be used. K_1 photons radiated directly from the primary target to the secondary target have a maximum angle of convergence of about 35°. Therefore, the actual K_1 photon distribution can be represented reasonably well by a collimated beam of photons entering the secondary target normal to its surface. In the following analysis it will be assumed that the incident beam is collimated and infinite in extent and that the secondary target is infinite in extent. It will be seen in the calculations that follow that this assumption is very good except at points near the edges of the target. The application of this analysis will underestimate the K_2 photon yield of the secondary target because the incident beam is not actually collimated. However, very near the target edges the analysis will overestimate the yield because the target is finite in extent. Whether these two opposing conditions will reduce the net error of the analysis to zero is doubtful; however, the errors do tend to cancel and it will be assumed here that they do cancel. The following analysis refers to Figure 7.

An infinite, monoenergetic, collimated beam of photons ϕ^* is attenuated according to the relation

$$\phi_1 = \phi^* e^{-\mu_1 a} \tag{37}$$

where μ_1 is the total attenuation coefficient of the photons in the

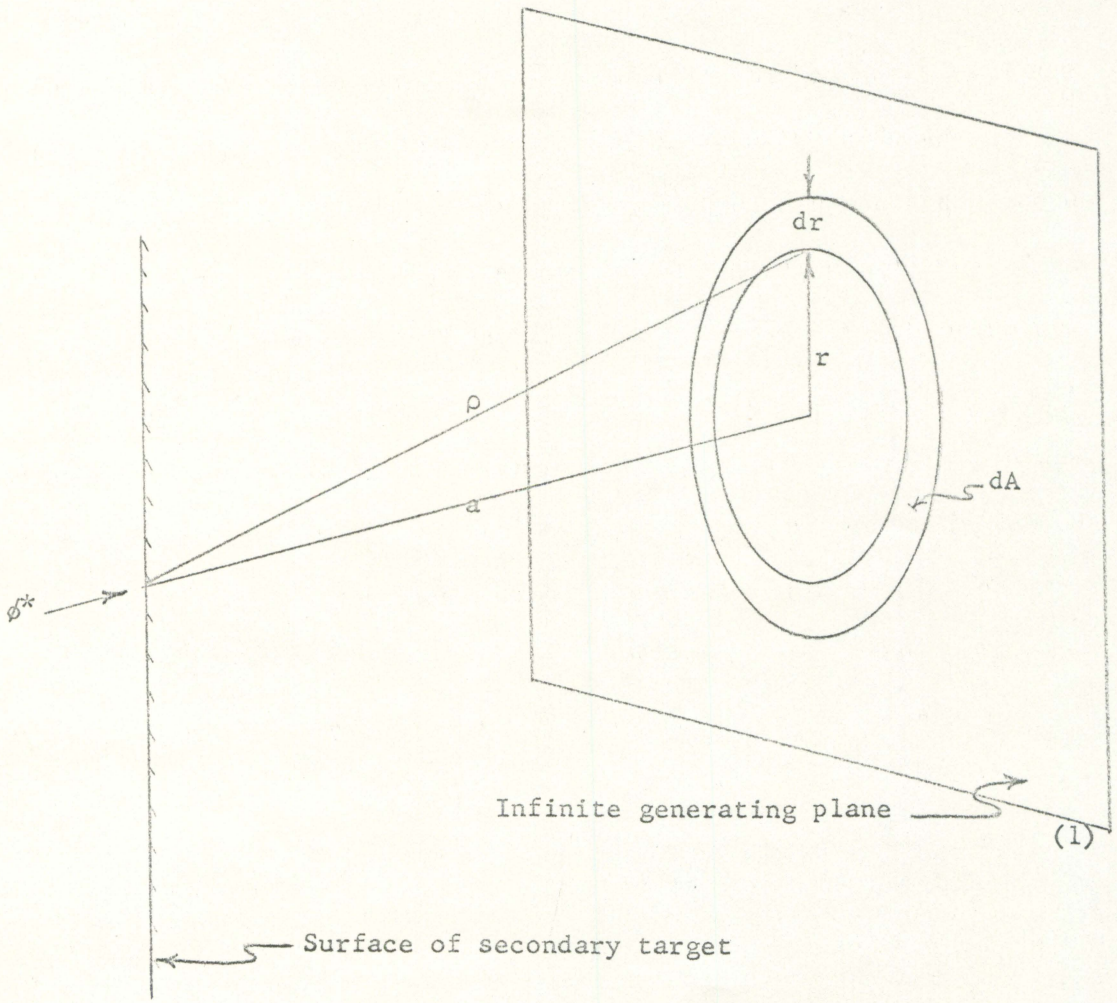

Figure 7. Geometrical arrangement used in the analysis of the secondary target

absorber, and a is the distance penetrated into the absorber. At point 1 in the secondary target, the area source term for isotropic production of K_2 photons due to photoelectric absorption of K_1 photons is

$$S_2 = W_k \mu_{1p} \phi_1 \, da \tag{38}$$

where da is the differential thickness of the volume source at point 1 and μ_{1p} is the photoelectric absorption coefficient for K_1 photons in the target. Since the incident beam is infinite in extent, this source term applies to an infinite plane which is parallel to the surface of the target and passes through point 1. The K_2 photon flux at the surface of the target due to the infinite plane source at point 1 is

$$\phi_2' = S_2 \int_{\rho=a}^{\infty} \frac{e^{-\mu_2 \rho}}{4\pi\rho^2} \, dA \tag{39}$$

where μ_2 is the total attenuation coefficient for K_2 photons. The expression for the differential area dA is

$$dA = 2\pi r \, dr \tag{40}$$

When dA is expressed in terms of ρ and substituted into Equation 39, the expression for ϕ_2' is

$$\phi_2' = S_2/2 \int_{a}^{\infty} \frac{e^{-\mu_2 \rho}}{\rho} \, d\rho \tag{41}$$

By making the definition

$$t = \mu_2 \rho \tag{42}$$

and substituting into Equation 41, the expression for ϕ_2' can be shown as

$$\phi_2' = S_2/2 \int_{b_2}^{\infty} \frac{e^{-t}}{t} \, dt \tag{43}$$

where $b_2 = \mu_2 a$.

The exponential integral in Equation 43 is defined as an $E_1(b)$ function in the literature. By substituting for the source term S_2, Equation 43 can be expressed as

$$\phi_2' = \frac{W_k \, \mu_{1p} \, \phi^*}{2} \, e^{-b_1} \, E_1(b_2) \, da \tag{44}$$

The total flux ϕ_2 due to K_2 photon generation over the whole target thickness is the integral of the above expression evaluated for all values of a. Since $E_1(b_2)$ is an improper integral, the total K_2 photon flux at the surface of the secondary target can be expressed as

$$\phi_2 = \frac{W_k \, \mu_{1p} \, \phi^*}{2} \sum_{a=\frac{\Delta a}{2}}^{\infty} e_a^{-b_1} \, E_1(b_2)_a \, \Delta a \tag{45}$$

The net K_2 photon yield of each of the three secondary target materials was calculated using Equation 45. Two intervals were used: Δa = 20 mg/cm^2 and Δa = 40 mg/cm^2. These two intervals yielded essentially the same results which indicates that the intervals were small enough to accurately evaluate the function.

Figure 8 is a plot of secondary target yield for each target material as a function of target thickness. Table 3 lists the infinite generating target thickness and maximum net K_2 photon yield for each material as

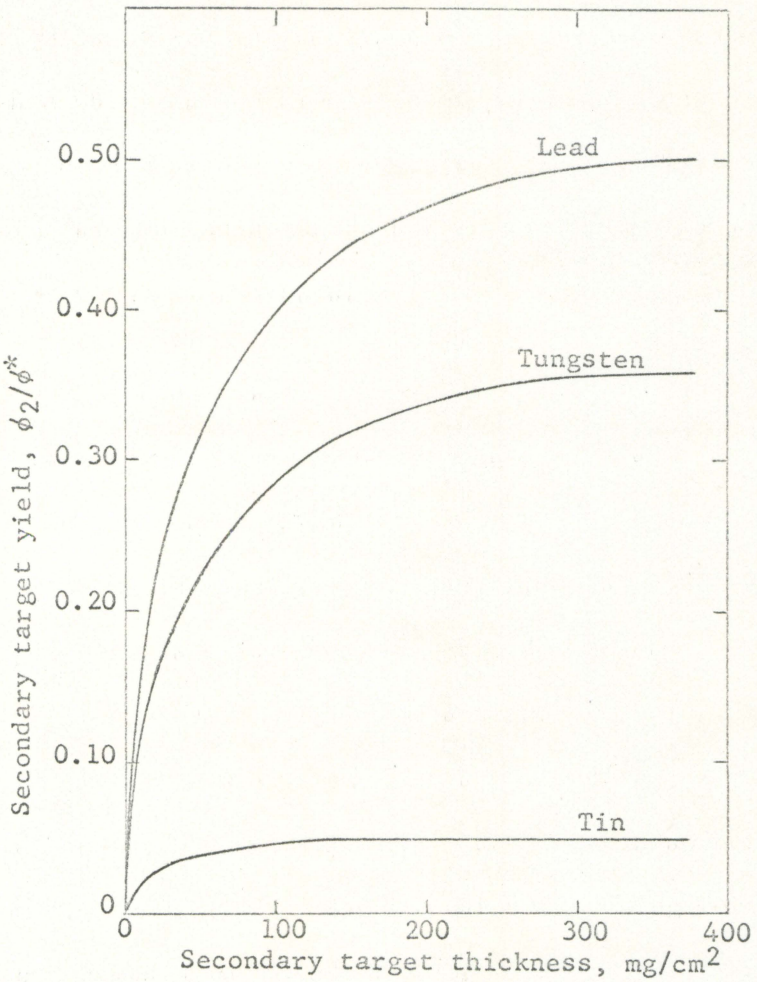

Figure 8. Secondary target yield as a function of target thickness

Table 3. Secondary target yield and thickness

Target	Thickness (mg/cm^2)	ϕ_2/ϕ^*
Lead (Pb)	350	0.50
Tungsten (W)	300	0.36
Tin (Sn)	150	0.05

determined by Equation 45.

No experimental results have been found with which to compare the results of this method of calculation. On a relative basis the results seem reasonable. Lead should be the most efficient K_2 photon generator and tin the poorest. It is to be expected that the contribution of each subsequent layer Δa to the total net K_2 photon flux at the target surface will be smaller than that of the preceding layer.

Calculations showed that a K_2 photon generating disk 380 mg/cm^2 from the surface of a lead target yielded 95 percent of the infinite plane contribution at that point when the radius of the disk was 1130 mg/cm^2. This corresponds to a linear radius of 0.1 cm. This same radius disk placed at a depth of 20 mg/cm^2 from the surface of the target yielded over 99 percent of the infinite plane contribution to ϕ_2' at that point. Thus it is seen that the infinite plane approximation made in this analysis is very good within 0.1 cm of the edges of the target.

Estimation of Source Strength

There are many possible applications for this type of device and each has its own geometrical and source strength requirements. In this design the source strength will be calculated for the case of a thickness gaging system employing a NaI scintillation detector and a differential pulse height analyzer. It will be assumed that the detector is one and one-half inches in diameter and is positioned 5 cm from the device along its axis of symmetry. The arrangement will be gaging low-density thin films with the 25.3 Kev X-rays generated by a tin target. The thickness of the films being gaged will be assumed to be two relaxation lengths. The arrangement of this system is shown in Figure 9.

In calculating the geometry for the system, the secondary target will be divided into three area elements, the centers of which are represented by the points A, B, and C. A geometry factor will be determined for the center of each element and applied to the whole element. Since the detector is not located on a cord of the sphere of emission of any element, an effective detector area must be calculated for each element. It will be assumed that the radius of the sphere of emission is the distance from the center of the detector to the center of the area element. The effective diameter of the detector is then the cord determined by the intercept of the surface of the sphere with the rays projected to the extremity of the detector from the point. In the case of the area element C, a portion of the detector is shadowed by the beta shield. Approximate calculations showed that only about 83 percent of the detector is seen at point C. The K_1 photon fluxes ϕ^* at points A, B, and C have already been calculated in the evaluation of Equation 34. The total K_2 photon flux ϕ_2 at the surface of the secondary target is emitted into a hemisphere from the target

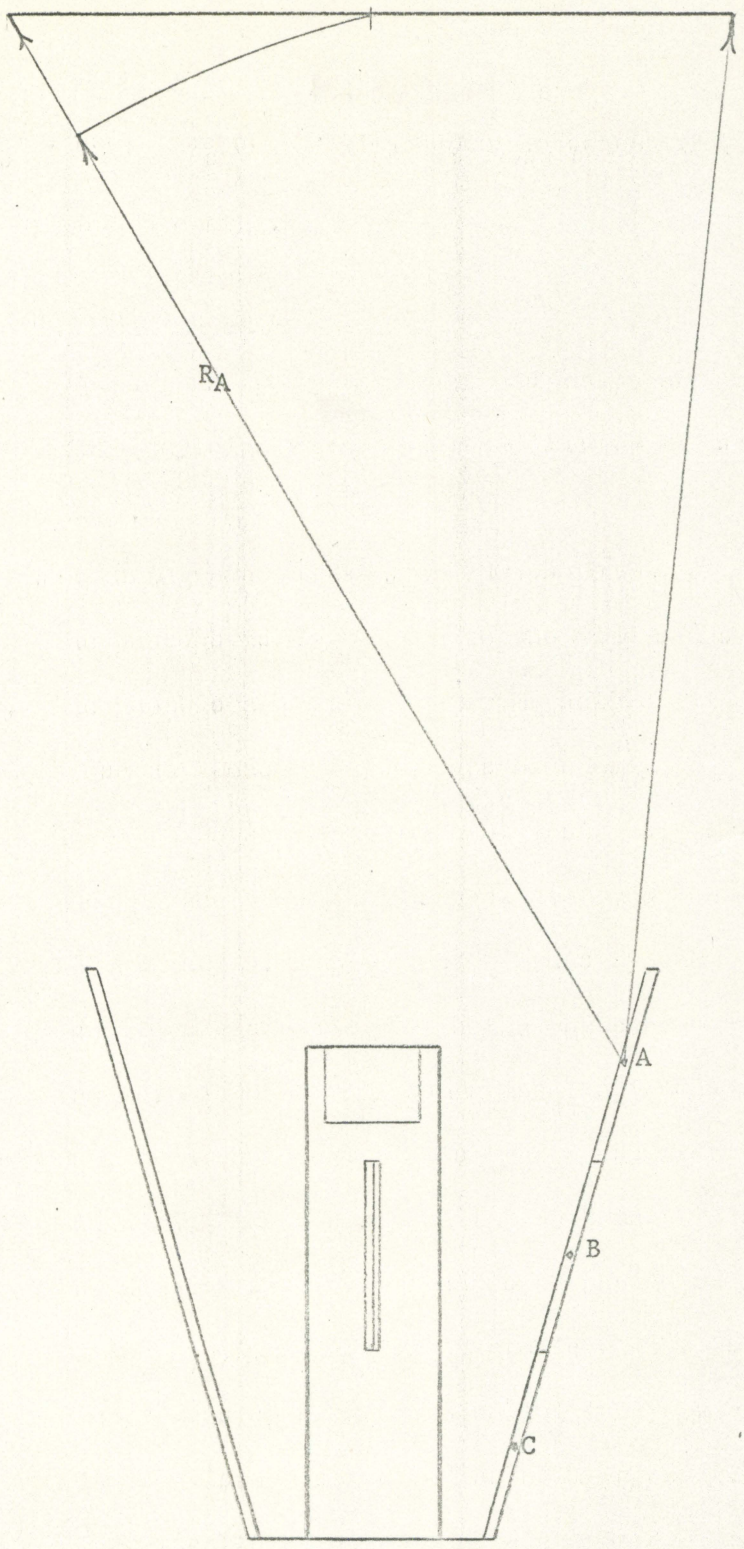

Figure 9. Source-detector arrangement. Scale: 1 inch = 1 centimeter

surface.

The geometry factors between each of the points and the detector are

$$G_A = \frac{A_{DA}}{2\pi R_A^2} = 0.047 \tag{46a}$$

$$G_B = \frac{A_{DB}}{2\pi R_B^2} = 0.037 \tag{46b}$$

$$G_C = \frac{A_{DC}}{2\pi R_C^2} = 0.027 \tag{46c}$$

where A_D at each point is the area of the detector seen at the point and R is the radius of the hemisphere of emission between the center of the detector and the point. The actual dimensions used in these calculations were scaled from Figure 9.

Each of the area elements has an altitude of one centimeter. By applying the equation for the area of the curved surface of a frustum of a right circular cone, the area of each of the elements is found to be

$$A_A = 8.5 \text{ cm}^2 \tag{47a}$$

$$A_B = 6.5 \text{ cm}^2 \tag{47b}$$

$$A_C = 4.6 \text{ cm}^2 \tag{47c}$$

The number of K_2 photons reaching the detector from area element A is

$$K_{2A} = \phi_A^* \frac{\phi_2}{\phi^*} A_A G_A e^{-\mu t} \tag{48}$$

Similar expressions are obtained for area elements B and C. In each case, ϕ_2/ϕ^* is the K_2 photon yield determined for tin, i.e., 0.05. Calculations showed that the photon attenuation in the air between the bottom

of the area element C and the detector was negligible. Therefore, the exponential attenuation term in Equation 48 is just the attenuation encountered in passing through two relaxation lengths of gaged material. Evaluation of Equation 48 for each of the three area elements yields

$$K_{2A} = 7.0 \times 10^{-5} S_L \tag{48a}$$

$$K_{2B} = 11.0 \times 10^{-5} S_L \tag{48b}$$

$$K_{2C} = 3.4 \times 10^{-5} S_L \tag{48c}$$

The total number of K_2 photons K_{2T} reaching the detector is the sum of the photons for each element.

$$K_{2T} = 2.14 \times 10^{-4} S_L \tag{49}$$

A simplified approximation of the previous calculations has been found to give good results for determining the yield of K_2 photons at the detector. In this approximation, the secondary target is replaced by a point isotropic source located at the intersection of the axis of symmetry of the device with the plane of the upper base of the frustum. Equation 35 is then applied to the whole secondary target to determine the intensity of the point source, and a geometry factor determined between the point and the detector by standard methods. This approximation applied to the present case underestimated the more detailed method by 23 percent.

In order to estimate the strength of source required in the present application, it will be assumed that 10^3 K_2 photons are required at the detector each second in order to provide a rapid response for the gaging

system. Therefore, the actual strength C of the source required is determined by this condition, Equation 49, and Equation 36.

$$C = 4.67 \times 10^7 \frac{\text{dis } Y^{90}}{\text{sec}} = 1.26 \text{ millicuries} \qquad (50)$$

In order to allow for assumptive errors, the source will be specified at 3.0 ± 0.5 millicuries of Y^{90}. Therefore, the actual intensity of the source will be

$$C = 11.1 \times 10^7 \frac{\text{dis } Y^{90}}{\text{sec}} \qquad (51)$$

Three millicuries of Sr^{90} are required to produce this amount of Y^{90} at equilibrium. Therefore, the total intensity of the source at equilibrium will be 6.0 millicuries. Calculations showed that 21 μg of Sr^{90} are required to provide this source intensity. Assuming that essentially carrier-free material is used, the line source geometry assumed at the beginning of this design can be approximated quite well.

Shielding Requirements

The shielding requirements of this device consist of a biological shield for protection of personnel and a primary shield to shield source radiation from the detector.

The effects of several types of radiation were investigated to determine the thickness of lead biological shielding required. It was found that K_1 photons were rapidly absorbed in the lead, but that the secondary radiation generated in the process required a considerably greater thick-

ness of shielding. This thickness was calculated to be 3.0 g/cm^2 to reduce the intensity of the secondary radiation to acceptable levels. High-energy bremsstrahlung was also investigated and proved to require the greatest amount of shielding. The following method of analysis was employed.

By utilizing the experimental results of Starfelt et al. (19), it is estimated that the yield of high-energy bremsstrahlung will be about 0.08 photons per beta decay in this design. The energy range of this radiation is from 100 Kev to 500 Kev. Above 500 Kev the intensity of radiation becomes negligibly small. In this calculation, an average photon energy of 200 Kev will be assumed; a build-up factor of 1.5 will then be applied to the calculation. The attenuation of 200 Kev photons in a tin target and the plastic housing will be small. The greatest intensity of 200 Kev photons along the face of the biological shielding will occur at a point opposite the midpoint of the source. By evaluating Equation 34 at this point it is found that the high energy photon flux ϕ_{ho} is

$$\phi_{ho} = \frac{S_{Li}}{4\pi(2)} \left[2F(15°,0.43)\right] = 1.2 \times 10^5 \qquad (52)$$

where $S_{Li} = 0.08$ C.

This flux will be assumed to be collimated as it passes through the shielding.

The energy absorbed in the air at the outer surface of the shielding is given by the relation

$$E_a = B\, \phi_{ho}\, e^{-\mu t}\, E\, \mu_a \qquad (53)$$

where B is the build-up factor, E is the energy of the radiation in Mev, and μ_a (cm^2/g) is the absorption coefficient for the radiation in air. When E_a is converted into a dose rate DR measured in milliroentgens per hour

$$DR = \frac{(3.6 \times 10^6)\ B\ \phi_{ho}\ E\ \mu_a}{5.5 \times 10^7}\ e^{-\mu t} \qquad (54)$$

where t is the thickness of the shielding. At $t = 4.5\ g/cm^2$, the dose rate due to high-energy bremsstrahlung is reduced to 0.7 mr/hr.

As the high-energy bremsstrahlung traverses the shielding it generates secondary radiation due to photoelectric absorption. The contribution of this secondary radiation to the dose rate at the outer surface of the shield can be calculated by using the same analysis that was employed in evaluating the primary target. The dose rate DR_S due to K-characteristic radiation generated in the shielding can be expressed for any thickness t by

$$DR_S = \frac{3.6 \times 10^6\ E\ \mu_a\ W_k\ \mu_{hp}\ \phi_{ho}}{5.5 \times 10^7\ (\mu_2 - \mu_h)}\ [e^{-\mu_h t} - e^{-\mu_2 t}] \qquad (55)$$

where μ_2 is the attenuation coefficient of the secondary radiation in the shielding, μ_h is the attenuation coefficient of the incident radiation, and μ_{hp} is the photo-absorption coefficient of the incident radiation. These coefficients all have units of cm^2/g. By evaluating the above equation for a thickness $t = 4.5\ g/cm^2$, DR_S is calculated to be 0.2 mr/hr. Therefore, the maximum dose rate in the air at the surface of a 0.5 cm

thick shield is 0.9 mr/hr. This amount is well within present permissible continuous exposure levels, so the biological shield will be specified at a thickness of 0.5 cm.

The function of the primary shield is to reduce the direct transmission of radiation from the primary target to the detector. On the basis of the previous calculations, a complete analysis of this shield is not necessary. It is felt that a thickness of 0.4 cm is sufficient to adequately shield the primary target from the detector.

In order to prevent damage to the biological shielding, the device will be covered with an aluminum shell. During normal operation a thin glass window will be placed over the output of the device and held in place by means of a threaded aluminum cap. This window will act as a dust cover and will also hold the secondary target in place. When not in operation, the window will be removed and replaced with a 0.5 cm thick lead disk shield.

No additional shielding will be included in the present design; however, it is felt that when the tin target is used, added shielding may be required. Over 70 percent of the K_1 photons incident upon a tin secondary target will be transmitted unattenuated to the face of the biological shield where an intense flux of characteristic radiation of the shield will be generated. The portion of this radiation received by the detector may be significant enough to warrant additional shielding. If such is the case, this shielding can be accomplished by placing an annulus of tin over the plastic housing and biological shield. A tin thickness of 0.3 cm would be sufficient to reduce the interference from

this source of radiation to negligible levels.

Effects of Compton Scattered Radiation

Throughout this design efforts have been made to maintain the purity of the useful radiation output. The primary target was optimized for the passage of K_1 photons. This means that 98 Kev photons generated by ionizing and radiative-collision processes will predominate in intensity over all other photon energies emitted by the primary target. This has been verified by Starfelt et al. (19), using Pr^{143} (E_{max} = 0.92 Mev) and Pr^{144} (E_{max} = 2.98 Mev) with tin and lead transmission targets. The majority of K_1 photons traversing the beta shield reach the secondary target unattenuated. Those that do interact with the beta shield are mostly scattered by Compton collisions. Those photons that scatter into the primary shielding will be almost completely absorbed, except for the high-energy bremsstrahlung whose intensity decreases rapidly with increasing energy. A large portion of the photons scattered into the secondary target will possess sufficient energy to undergo photoelectric absorption in the target. Unless the energies of scattered K_1 photons are less than the K absorption edge of the target, they will have a higher probability of undergoing photoelectric absorption than those K_1 photons transmitted to the secondary target unattenuated. The thickness of the secondary target was optimized so that a near maximum number of K_2 photons would be produced at its surface. However, the underlying reason for this optimization was to keep the target as thin as possible in order to minimise Compton scattering of the incident radiation. All of the above

considerations are important in maintaining the homogeneity of the useful radiation output.

A complete analytical analysis of the effects of Compton scattering upon the useful radiation output of this device would comprise a separate study in itself. Such an analysis would have to consider the effects of geometry, material placement and thickness, and multiple scattering. For the purpose of estimating the magnitude of one of the more dominant sources of Compton scattered radiation in this design, a simple analysis can be employed.

Since K_1 photons incident upon the secondary target predominate in number over the photons at any other energy, an estimation of their contribution to the useful radiation output would also estimate the upper limit of the contribution in any other energy region. This excludes the energy region from zero to 10 Kev where the effects of L shell ionization processes become significant. In the following analysis a lead secondary target will be assumed.

As K_1 photons traverse the secondary target they generate Compton scattered photons in numbers which are proportional to the K_1 photon flux distribution in the target. It will be assumed that the Compton scattered photons have an isotropic distribution in the target; for 98 Kev photons this assumption is not bad. By making this assumption, it is possible to treat the Compton scattering of K_1 photons in exactly the same manner as the production of K_2 photons was treated in the analysis of the secondary target. The only thing preventing direct application of the results of the analysis of the secondary target is the fact that

in the present case the $E_1(b)$ function is dependent on the scattering angle of the K_1 photons, while in the analysis of the lead secondary target the $E_1(b)$ function was evaluated for 75 Kev photons. Compton scattered K_1 photons will have energies ranging from near 98 Kev to about 70 Kev. In the present analysis it will be assumed that the $E_1(b)$ function for 75 Kev photons can be used and the effects of this assumption evaluated in the results. By utilizing the above assumptions, the ratio of the Compton scattered K_1 photon flux ϕ_{1c} to the total K_2 photon flux ϕ_2 at the surface of the secondary target is

$$\frac{\phi_{1c}}{\phi_2} = \frac{\mu_{1c}}{W_k \mu_{1p}} \tag{56}$$

where μ_{1c} is the Compton scattering probability of the incident K_1 photons. By assuming isotropic scattering of K_1 photons, the detector will intercept these photons in the same proportion as given by the above equation. When Equation 56 is evaluated for a lead target, it is found that $\phi_{1c}/\phi_2 = 0.02$. Thus, for a lead secondary target, the contribution of Compton scattered K_1 photons to the spectrum of the useful radiation output is expected to be about two percent of the peak intensity of the K_2 photon output. This is an order of magnitude lower than Filosofo (7) experimentally determined for a Y^{90} source using a lead target in transmission geometry.

In Figure 9 the average scattering angles of K_1 photons scattered from points A, B, and C into the detector are the following: A, 65° (88 Kev); B, 97° (80 Kev); and C, 149° (72 Kev). The energies associated with each angle are the energies of the scattered photons. Thus it is

seen that at point A the scattered photons will have a very high probability of being photoelectrically absorbed before escaping the target, so Equation 56 will overestimate the actual contribution of Compton scattered K_1 photons from this region. At point B, Equation 56 underestimates the contribution of scattered K_1 photons because the attenuation coefficient which applies to this energy radiation is less than that assumed by the equation. At point C, Equation 56 overestimates the contribution of scattered K_1 photons because the attenuation coefficient which applies to this energy radiation is greater than that assumed by the equation. Therefore, even though the reasoning which led to the development of Equation 56 is an oversimplification of very complex phenomena, it is felt that this method of evaluation yields results which are at least of the proper order of magnitude.

SUMMARY

Figure 10 shows a full scale cross-sectional view of the X-ray device as it was designed in this investigation. Since the device was designed for general applications, its size can be considered to be somewhat arbitrary. Specific applications would necessitate certain modifications to meet individual requirements; however, the basic considerations included in this design could be applied directly to any application.

The analysis of the primary target was made independently of past semitheoretical approaches. Although it was found that the results of this analysis have already been reported in the literature, the approach utilized in this design verified the validity of this type of analysis for a range of beta emitters and target materials.

The analysis of the secondary target was based upon an extension of the exponential kernel method of calculation, and no similar approach to this type of problem has been found in the literature. In addition, no experimental results have been found with which to compare this method of calculation. For these reasons, the justification for using this type of analysis must be based upon the logic employed in its development and the reasonableness of the results obtained.

The method utilized in estimating the effects of Compton scattered radiation in a lead secondary target is based upon the analysis of the secondary target. This method was developed for one special case and should only be used to estimate relative magnitudes of scattering effects.

It is felt that some of the areas examined in this design could in

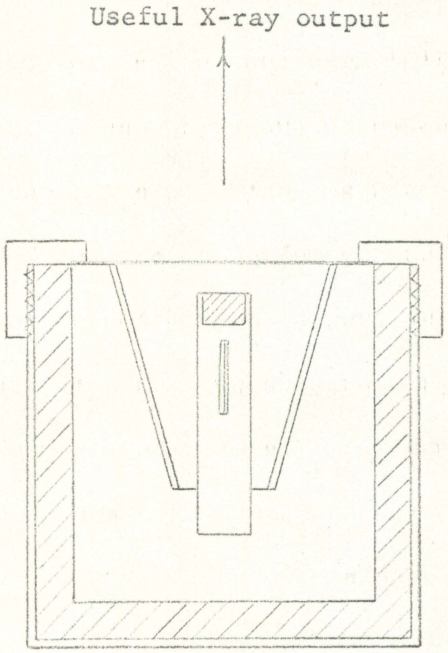

Figure 10. Full scale cross-sectional view of the X-ray device

themselves be expanded into more general investigations. With the increased utilization of isotopic sources of secondary radiation, the development of simplified methods of treating the complex interactions associated with such radiation sources would greatly facilitate their adaptation to new areas of application.

CONCLUSION

Based upon this investigation, it is felt that the beta-ray-excited X-ray device developed in this design can generate a useful radiation output which is considerably more homogeneous than that of the devices which have been evaluated to date. The useful radiation output of this device is not limited to a single energy, but can provide radiation covering a spectrum of energies simply by employing different secondary target materials. A device of this nature could be applied to a wide range of applications.

BIBLIOGRAPHY

1. Burtt, Benjamin P. Absolute beta counting. Nucleonics 5, No. 8: 28-43. August, 1949.

2. Cameron, J. F. and Rhodes, J. R. Beta-excited characteristic X-rays as energy reference sources. International Journal of Applied Radiation and Isotopes 7: 244-250. 1960.

3. Crouthamel, C. E., ed. Applied gamma-ray spectrometry. New York, N. Y., Pergamon Press. 1960.

4. Davisson, Charlotte Meaker and Evans, Robley D. Gamma-ray absorption coefficients. Reviews of Modern Physics 24: 79-107. 1952.

5. Evans, Robley D. The atomic nucleus. New York, N. Y., McGraw-Hill Book Company, Inc. 1955.

6. Fano, U. Gamma-ray attenuation. Nucleonics 11, No. 8: 8-12. August, 1953.

7. Filosofo, I. Isotopic sources of secondary radiation. U. S. Atomic Energy Commission Report ARF 1122-27. (Illinois Inst. of Tech., Chicago. Armour Research Foundation) 1961.

8. Gleason, G. I., Taylor, J. D., and Tabern, D. L. Absolute beta counting at defined geometries. Nucleonics 8, No. 5: 12-21. May, 1951.

9. Grodstein, Gladys White. X-ray attenuation coefficients from 10 kev to 100 mev. U. S. National Bureau of Standards Circular 583. 1957.

10. Kaplan, Irving. Nuclear physics. 2nd ed. Reading, Mass., Addison-Wesley Publishing Company, Inc. 1963.

11. Katz, L. and Penfold, A. S. Range-energy relations for electrons and the determination of beta-ray end-point energies by absorption. Reviews of Modern Physics 24: 28-44. 1952.

12. Leboeuf, M. B. and Stark, B. T. Excitation of characteristic X-rays by beta-particles. U. S. Atomic Energy Commission Report HW-31961. (Hanford Atomic Products Operation, Richland, Wash.) 1954.

13. Lidén, K. and Starfelt, N. Characteristic X-rays from thick β-ray sources. Arkiv För Fysik 7: 193-196. 1954.

14. McGinnies, Rosemary T. X-ray attenuation coefficients from 10 kev to 100 mev. U. S. National Bureau of Standards Supplement to Circular 583. 1959.

15. Reiffel, L. Beta-ray-excited low-energy X-ray sources. Nucleonics 13, No. 3: 22-24. March, 1955.

16. Rockwell, Theodore, III, ed. Reactor shielding design manual. New York, N. Y., D. Van Nostrand Company, Inc. 1956.

17. Segrè, E., ed. Experimental nuclear physics. Vol. 1. New York, N. Y., John Wiley and Sons, Inc. 1953.

18. Siegbahn, Kai, ed. Beta- and gamma-ray spectroscopy. New York, N. Y., Interscience Publishers, Inc. 1955.

19. Starfelt, N., Cederlund, J., and Lidén, K. The yield of characteristic X-rays excited by β-rays. International Journal of Applied Radiation and Isotopes 2: 265-273. 1957.

20. Voyvodic, L. Isotopic sources of secondary radiation. U. S. Atomic Energy Commission Report ARF 1122-13. (Illinois Inst. of Tech., Chicago. Armour Research Foundation) 1959.

21. Voyvodic, Louis and Stone, C. A. Isotopic sources of secondary radiation. U. S. Atomic Energy Commission Report AECU-4085. (Technical Information Service Extension, AEC) 1959.

ACKNOWLEDGMENTS

I wish to express my sincere appreciation to Dr. Glenn Murphy, head of the Department of Nuclear Engineering, for making this investigation possible, and for his continued counsel and encouragement.

I also wish to thank Mr. Donald S. Sasscer, Assistant Professor of Nuclear Engineering, for his constructive criticisms of portions of this design problem.